Supporting Information

Enhancing Cycling Stability of Lithium Metal Batteries by A Bifunctional Fluorinated Ether

Thanh-Nhan Tran, Xia Cao, Yaobin Xu, Peiyuan Gao, Hui Zhou, Fenghua Guo, Kee Sung Han, Dianying Liu, Phung ML Le, J. Mark Weller, Mark H. Engelhard, Chongmin Wang, M. Stanley Whittingham, Wu Xu*, and Ji-Guang Zhang*

Thanh-Nhan Tran, Xia Cao, Dianying Liu, Phung ML Le, J. Mark Weller, Mark H. Engelhard, Wu Xu, Ji-Guang Zhang
Energy and Environmental Directorate, Pacific Northwest National Laboratory, Richland, WA 99354, USA
wu.xu@pnnl.gov, jiguang.zhang@pnnl.gov

Yaobin Xu, Chongmin Wang
Environmental and Molecular Sciences Laboratory, Pacific Northwest National Laboratory, Richland, WA 99354, USA

Peiyuan Gao, Kee Sung Han
Physical and Computational Sciences Directorate, Pacific Northwest National Laboratory, Richland, WA 99354, USA

Hui Zhou, Fenghua Guo, M. Stanley Whittingham
Department of Chemistry, State University of New York at Binghamton, Binghamton, NY 13902, USA

Computational Details

CMD simulation

Three electrolyte systems, LiFSI-1.15DME-3BTFEE, LiFSI-1.2DME-3BTFEE, and LiFSI-1.2DME-3TTE, were investigated by classical molecular dynamics (CMD) simulation. The parameters of the FSI anion were obtained from the CL&P force field.[1] The parameters of Li ions were obtained from Dang's work.[2] The interaction parameters of other solvents and diluents were obtained from optimized potentials for liquid simulations (OPLS) force fields.[3,4] The F and H interaction parameters[5] were tuned to improve the excess volume and interfacial enthalpies of fluorinated ether.

To include the electronic polarizability effect, the partial charges of ions were treated by the electronic continuum correction (ECC) method.[6]

$$q_i^{eff} = \frac{q_i}{\sqrt{\varepsilon_\infty}} \quad (1)$$

where, ε_∞ is the high-frequency contribution to the solvent permittivity stemming from electronic fluctuations in the solvent molecules. It is be related to the refractive index n as

$$\varepsilon_\infty = n^2 \quad (2)$$

The refractive indices of solvents are listed in Table S1. The refractive indices of DME-BTFEE mixtures were calculated by Arago-Biot approach.[7] The effect of TTE diluent on DME is not considered in this study.

Table S1. The refractive indices of solvents

Solvent	Refractive index
DME	1.378[8]
BTFEE	1.3202[9]

All the CMD simulations were carried out with the GROningen Machine for Chemical Simulations (GROMACS) simulation package. Initially, the molecules and ions are randomly

inserted into the simulation box. The steepest descent method was used to minimize the energy of the systems. The systems were pre-equilibrated in an isothermal-isobaric (NPT) ensemble with 10 ns at 298 K and 1 bar. The temperature and pressure were controlled by a V-rescale thermostat[10] and a Berendsen barostat[11] with a time constant of 0.2 and 1 ps, respectively. Then 200 ns production simulations were performed at 298K in the canonical (NVT) ensemble. The temperature was controlled by the Nose-Hoover themostat[12] with a time constant of 0.2 ps. The cutoff of the Lennard-Jones potential is 1.2 nm. The particle mesh Ewald method[13] with a Fourier spacing of 0.15 nm and a 1.2 nm real-space cutoff is used for calculating electrostatic interactions. Periodic boundary conditions were used in all three directions. The time step is 2 fs. The bonds between H and other atoms were constrained by the LINCS algorithm.[14] The last 50 ns of trajectory data were used for data analysis. The snapshot was visualized by VMD.[15]

AIMD simulation

To investigate the relationship between the solvation structure and the electrochemical stability of the LiFSI-DME-BTFEE electrolyte, an *ab initio* molecular dynamics (AIMD) simulation was performed. The molar ratio is 1:1.2:3 in the AIMD simulation. The simulation approach is consistent with the methodology adopted in our prior research.[16]

DFT calculation

Density functional theory (DFT) calculations were performed using the B3LYP functional with the NWChem software.[17] The geometries were optimized with 6-31G** basis. Single point energy calculations were performed using 6-311++G** basis set. Vibrational frequencies were calculated for yielding zero-point energy and thermal corrections. Gibbs free energies were calculated at 298.15 K. An effect of implicit solvent with dielectric properties of acetone (dielectric constant=20) was included via Conductor-like Screening Model (COSMO) model.[18] Note that the binding energy calculations were based on one Li ion and one solvent molecule.

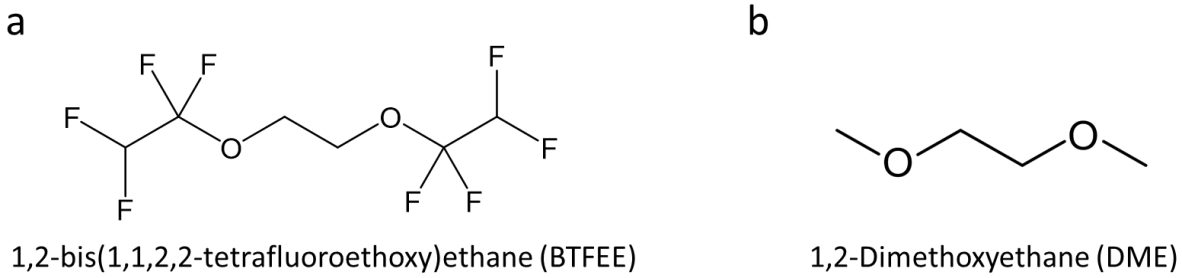

Figure S1. Chemical structures of (a) BTFEE and (b) DME.

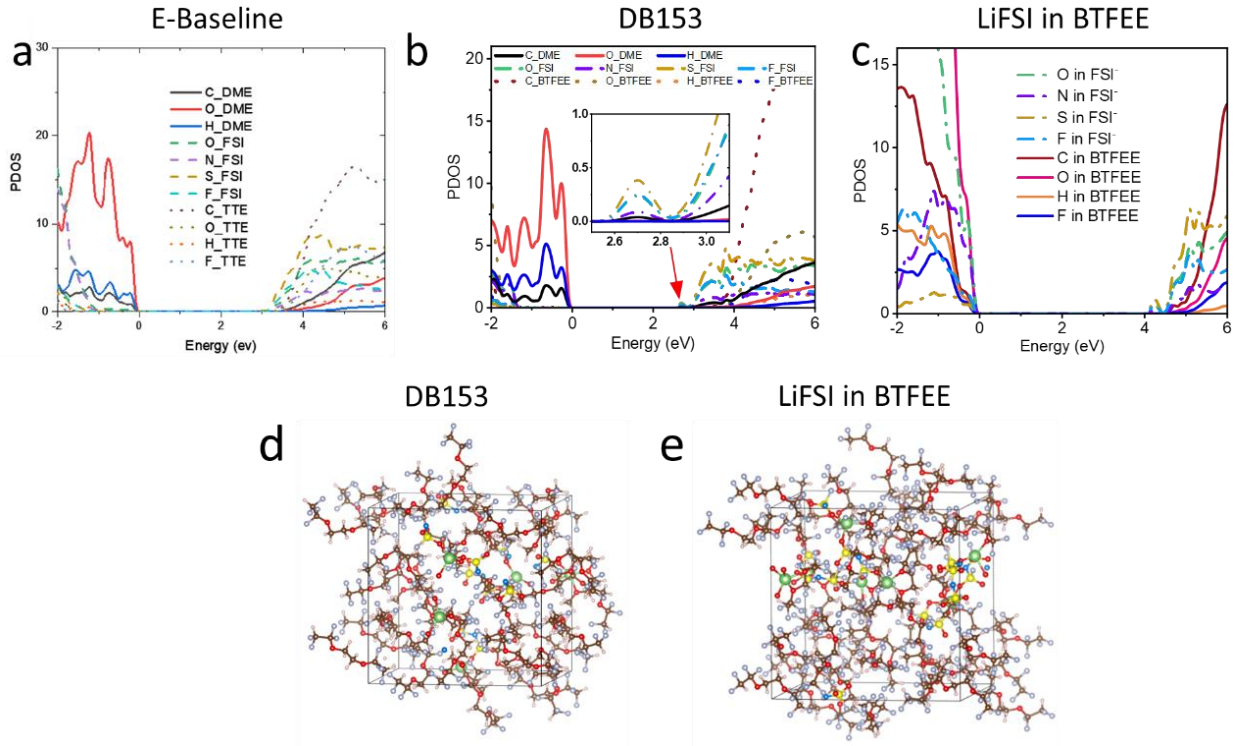

Figure S2. The projected density of state analysis of (a) E-Baseline,[16] (b) DB203 and (c) LiFSI in BTFEE (with 1:3 molar ratio) systems; AIMD simulation snapshots of (d) DB153 and (e) LiFSI in BTFEE (1:3) electrolyte systems. Color code: Li-green, C-brown, O-red, H-white, N-blue, F-pink, S-yellow.

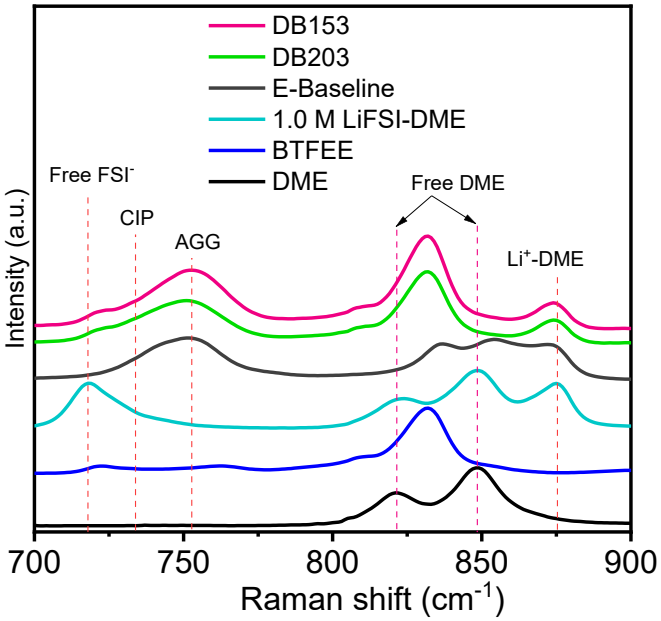

Figure S3. Raman spectra of DB153, DB203, E-Baseline, 1M LiFSI in DME, BTFEE and DME solvent.

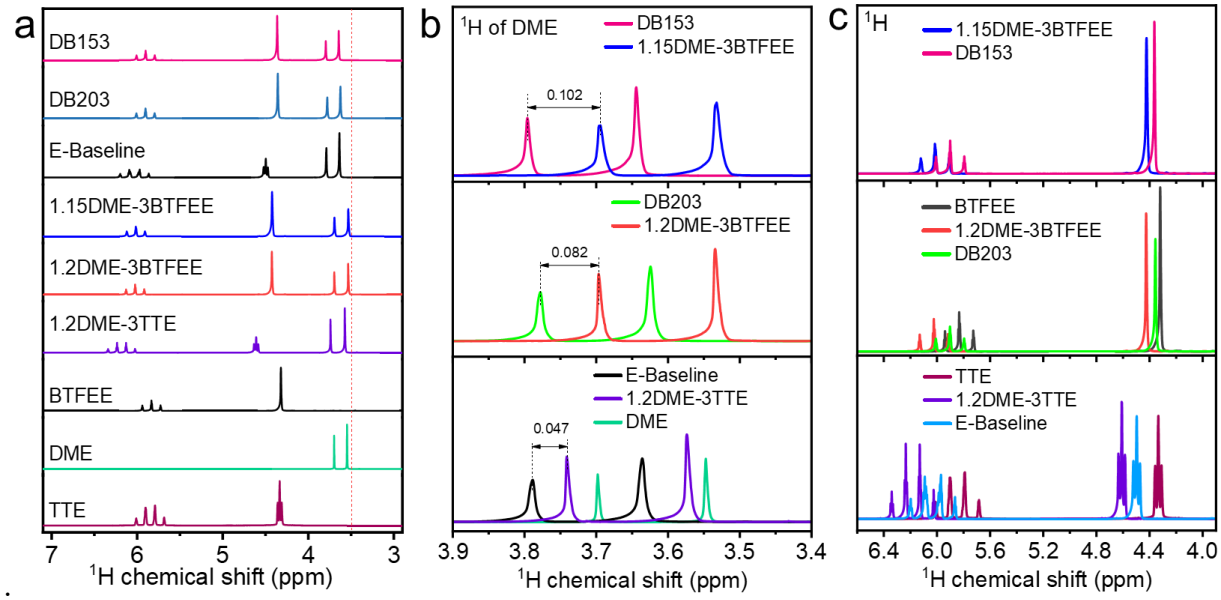

Figure S4. (a) ^{1}H NMR full spectra of all solvents and electrolytes; ^{1}H NMR spectra in (b) DME solvent region and (c) in diluents region of E-Baseline, DB203, DB153, 1.2DME-3TTE, 1.2DME-3BTFEE, 1.15DME-3BTFEE, DME, TTE and BTFEE.

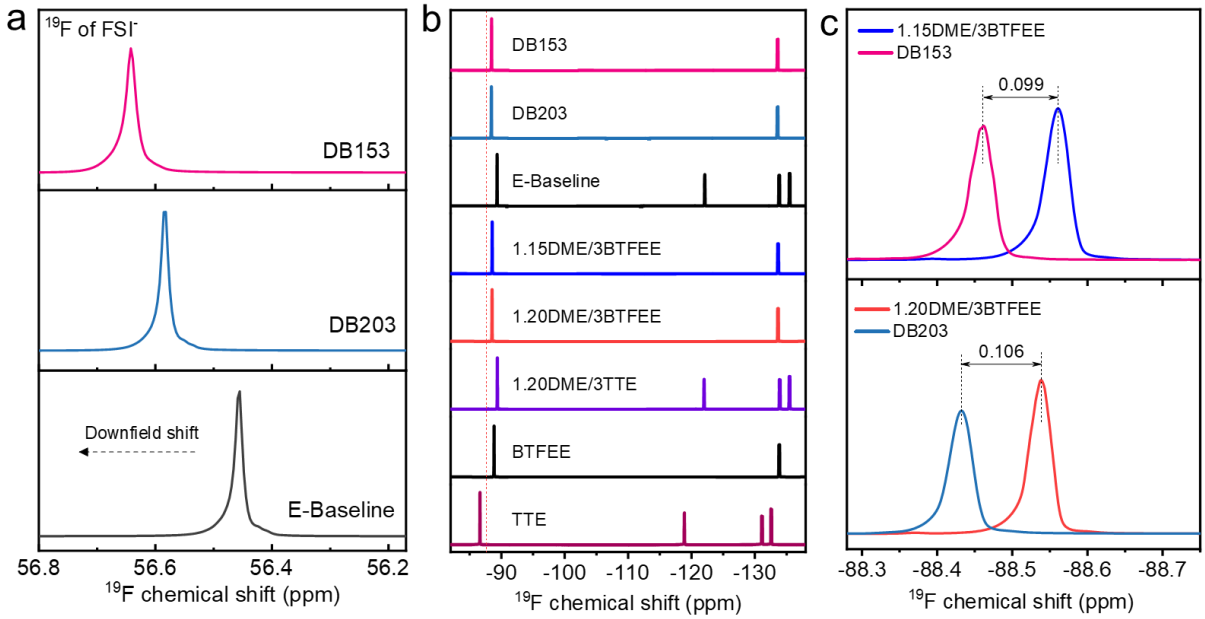

Figure S5. (a) ^{19}F NMR spectra in FSI$^-$ anion of DB153, DB203 and E-Baseline; (b) ^{19}F NMR full spectra of DB153, DB203, E-Baseline electrolytes, BTFEE, TTE solvent, 1.15DME/3BTFEE, 1.2DME/3BTFEE, 1.2DME/3TTE and (c) high resolution in diluents region of DB153, DB203, 1.15DME/3BTFEE, and 1.2DME/3BTFEE.

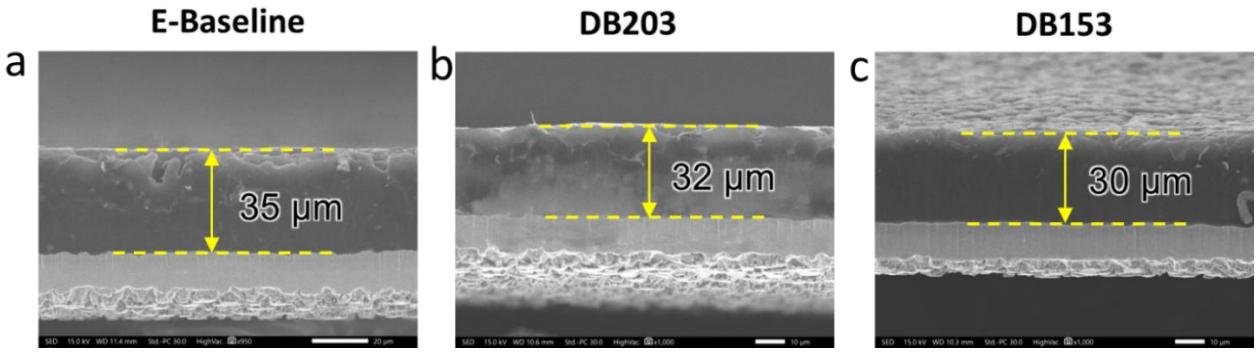

Figure S6. Cross-sectional SEM images of plated Li on Cu foils at the first time in (a) E-Baseline, (b) DB203 and (c) DB153.

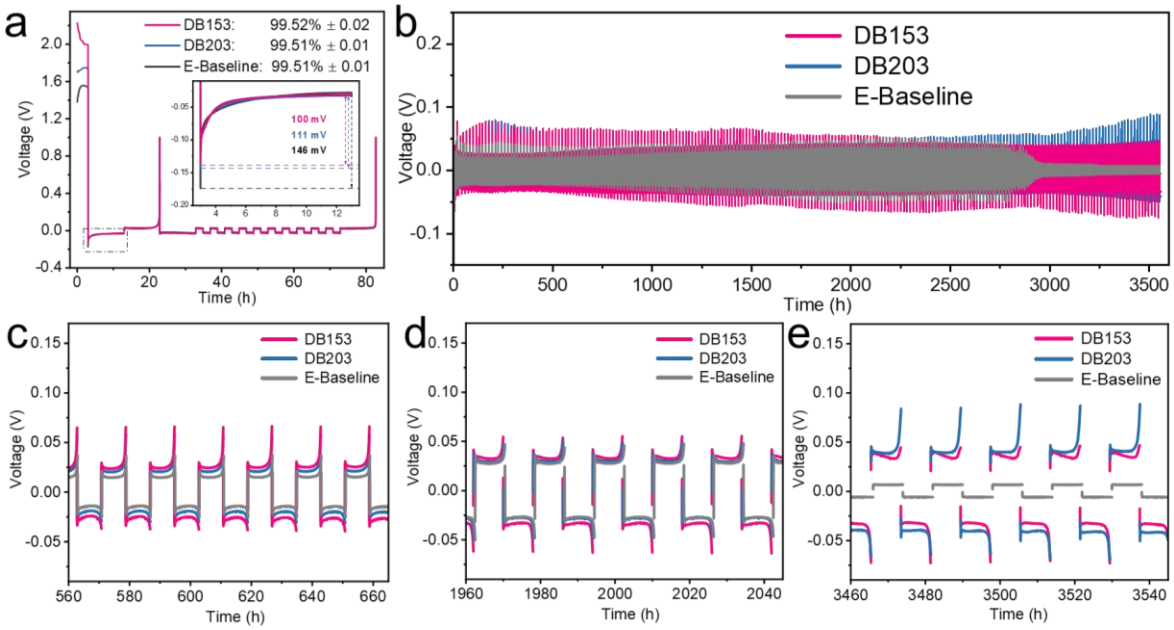

Figure S7. Electrochemical stability of Li metal in different electrolytes: (a) Li Coulombic efficiency in Li||Cu cells with modified Aurbach method, (b) long term voltage profiles of Li||Li symmetric cells; (c-e) the enlarged voltage profiles during different time ranges (highlighted region in (b)).

Table S2. Summary of the performances of recently reported electrolytes for LMBs.

Cathode	Cathode loading	Electrolyte	Voltage (V)	Initial capacity, capacity retention, and C-rate	Ref.
NMC811	**4.0 mAh cm^{-2}**	**LiFSI-1.15DME-3BTFEE**	**2.8 – 4.4**	**80% after 470 cycles at 0.1C charge/0.33C discharge**	**This work**
NMC811	8mg cm^{-2}	2M LiFSI-5TFDOL-5DME	3.0 – 4.4	94.5% after 220 cycles at 1C	*ACS Energy Lett.* **2023**, *0*, 3180.
NMC811	1.5 mAh cm^{-2}	1M LiFSI-1.2DME-3TFEO	2.8 – 4.4	80% after 300 cycles at C/3	*Nat. Energy* **2019**, *4*, 796.
NMC811	1.5 mAh cm^{-2}	LiFSI-1.0DME-3TTE	2.8 – 4.4	87.5% after 300 cycles at C/3	*Proc. Natl. Acad. Sci.* **2020**, *117*, 28603.
NMC811	1.6 mAh cm^{-2}	1.8M LiFSI in DPE	2.5 – 4.3	80% after 210 cycles at C/3	*Nat. Commun.* **2023**, *14*, 868.
NMC811	0.96 mAh cm^{-2}	LiFSI-1.2DME-3DFEB	2.8 – 4.2	80% after 250 cycles at 0.2C/0.5C	*ACS Nano* **2024**, *18*, 1969.
NMC811	1.5 mAh cm^{-2}	LiFSI-1.2DME-3TFEO	2.8 – 4.4	80% after 210 cycles at C/3	*Energy Storage Mater.* **2021**, *34*, 76.
NMC811	4.9 mAh cm^{-2}	1.5M LiFSI in F5DEE	2.8 – 4.4	80% after 200 cycles at 0.2C/0.3C	*Nat. Energy* **2022**, *7*, 94.
NMC811	0.25 mAh cm^{-2}	1 M LiTFSI/TMS + FEC (8:2, v/v)	2.7 – 4.4	86.1% after 500 cycles at 0.5C	*Energy Storage Mater.* **2022**, *44*, 527.
NMC811	4 mAh cm^{-2}	LiFSI-0.1FEC-1.4DME-TTE + 1% LiDFOB	2.7 – 4.3	80% after 200 cycles at 0.5C/1C	*Small* **2023**, *19*, 1.
NMC811	1.24 mAh cm^{-2}	2M LiFSI in BTFD:DME (1/1, v/v)	2.7 – 4.3	80% after 200 cycles at 0.3C	*Energy Storage Mater.* **2024**, *69*, 103375

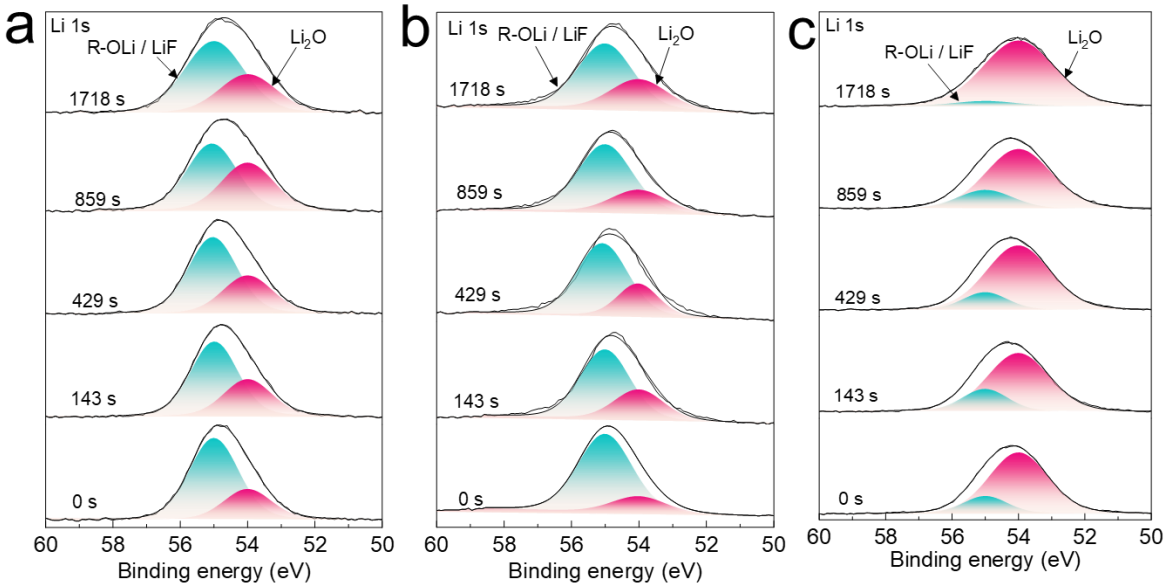

Figure S8. Reconstructed Li 1s XPS spectra after successive sputtering steps of the anode SEI in the full cells with (a) E-Baseline, (b) DB203 and (c) DB153 electrolytes.

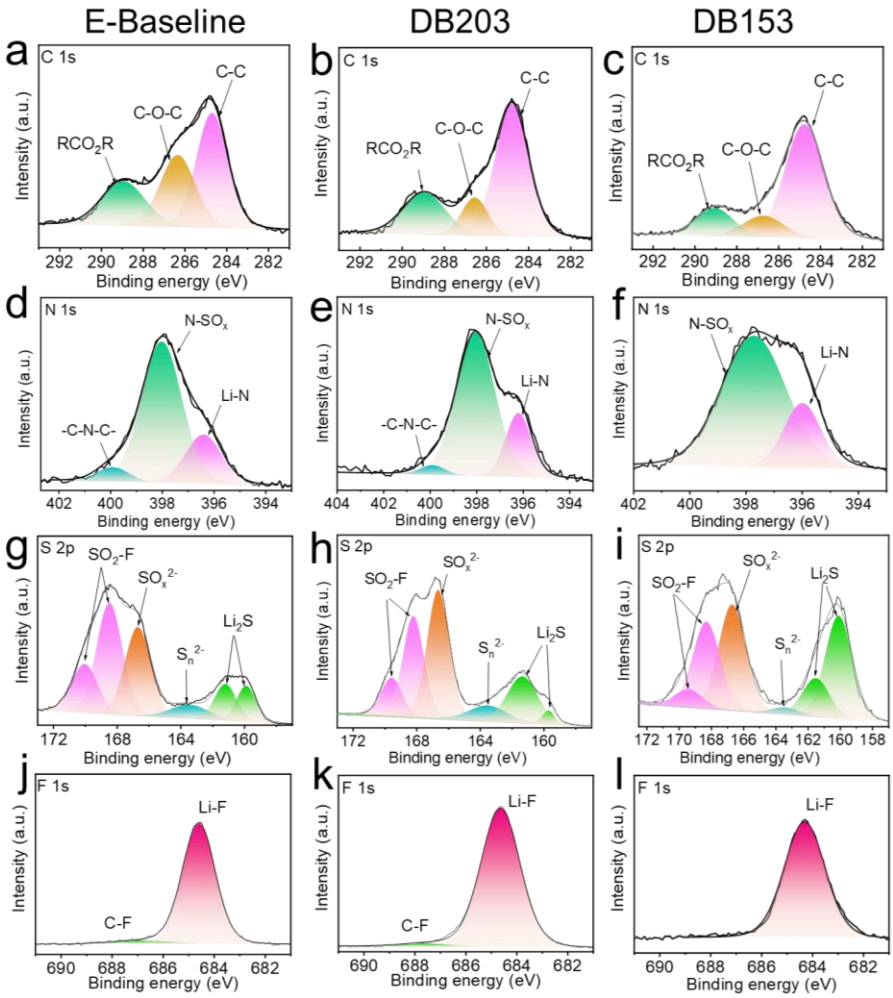

Figure S9. Reconstructed XPS spectra of SEI layer on cycled Li metal anode Li||NMC811 full cells after 150 cycles for (a-c) C 1s, (d-f) N 1s, (g-i) S 2p, and (j-l) F 1s for E-Baseline, DB203 and DB153, respectively.

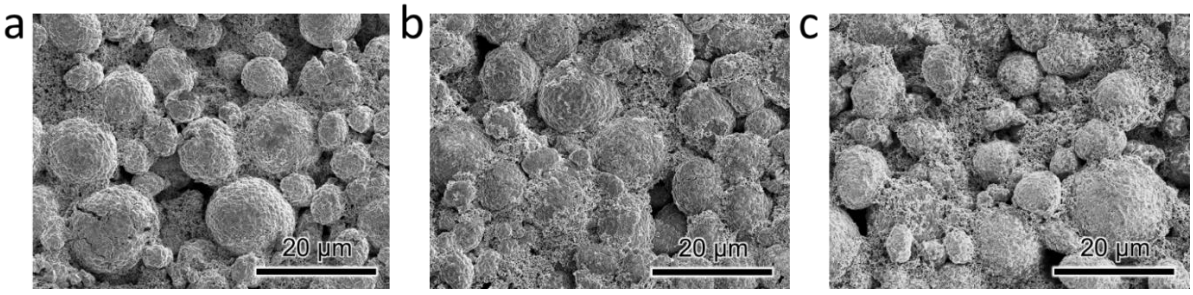

Figure S10. SEM top-view images of the cycled NMC811 after 150 cycles for (a) E-Baseline, (b) DB203, and (c) DB153 electrolytes.

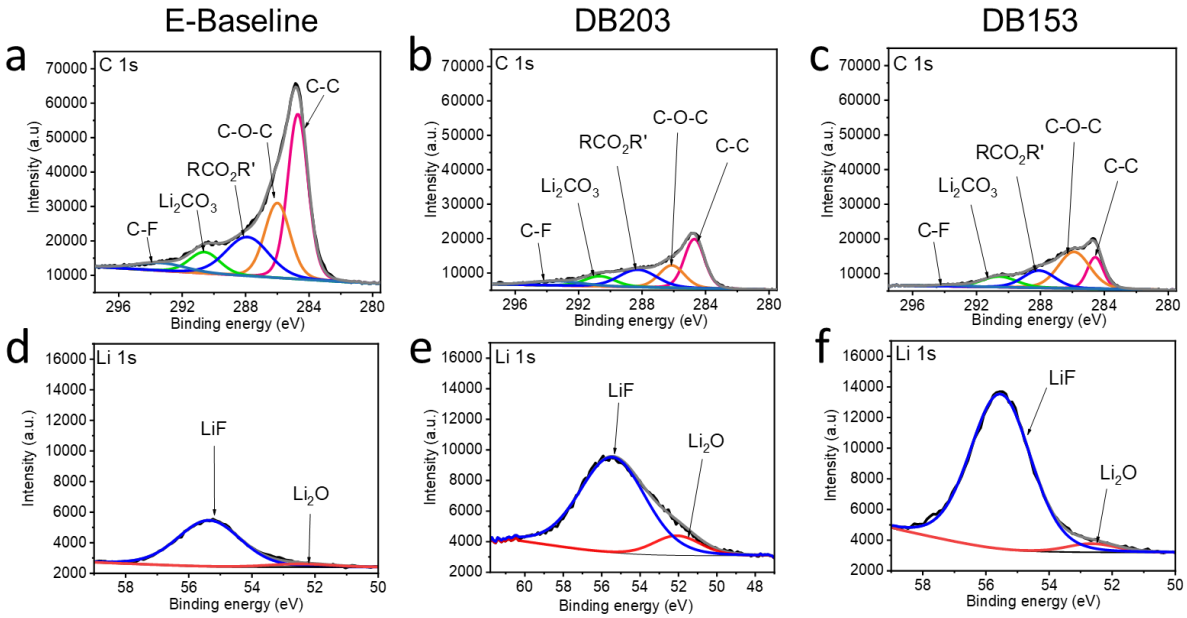

Figure S11. Reconstructed XPS spectra of CEI layer on cycled NMC811 cathode in Li||NMC811 full cells after 150 cycles for (a-c) C 1s, and (d-f) Li 1s for E-Baseline, DB203 and DB153, respectively

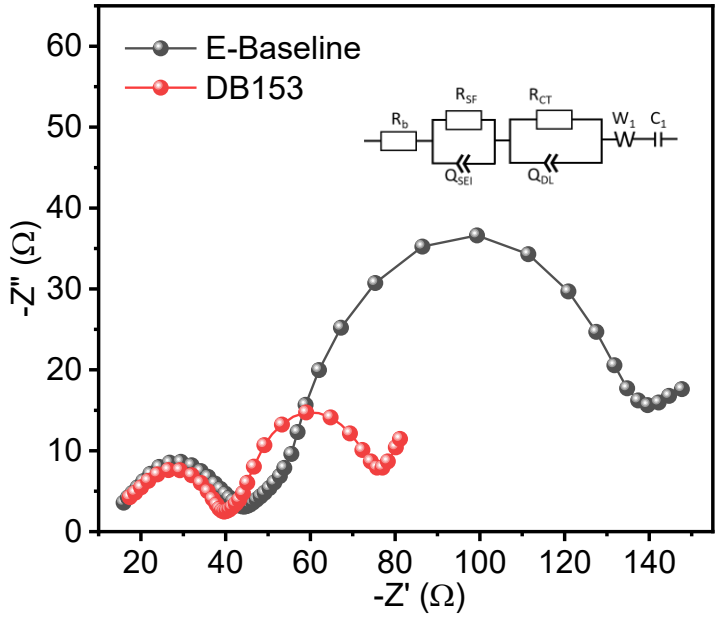

Figure S12. Nyquist plot of E-baseline and DB153 after 470 cycles at 50% state-of-charge. Inset shows the equivalent circuit for fitting.

Table S3. Summary of the fitted parameters for Nyquist plots in Figure S10.

Sample	Rb (Ω)	RSF (Ω)	RCT (Ω)
E-Baseline	11.3	36.6	100.0
DB153	13.4	28.0	35.6

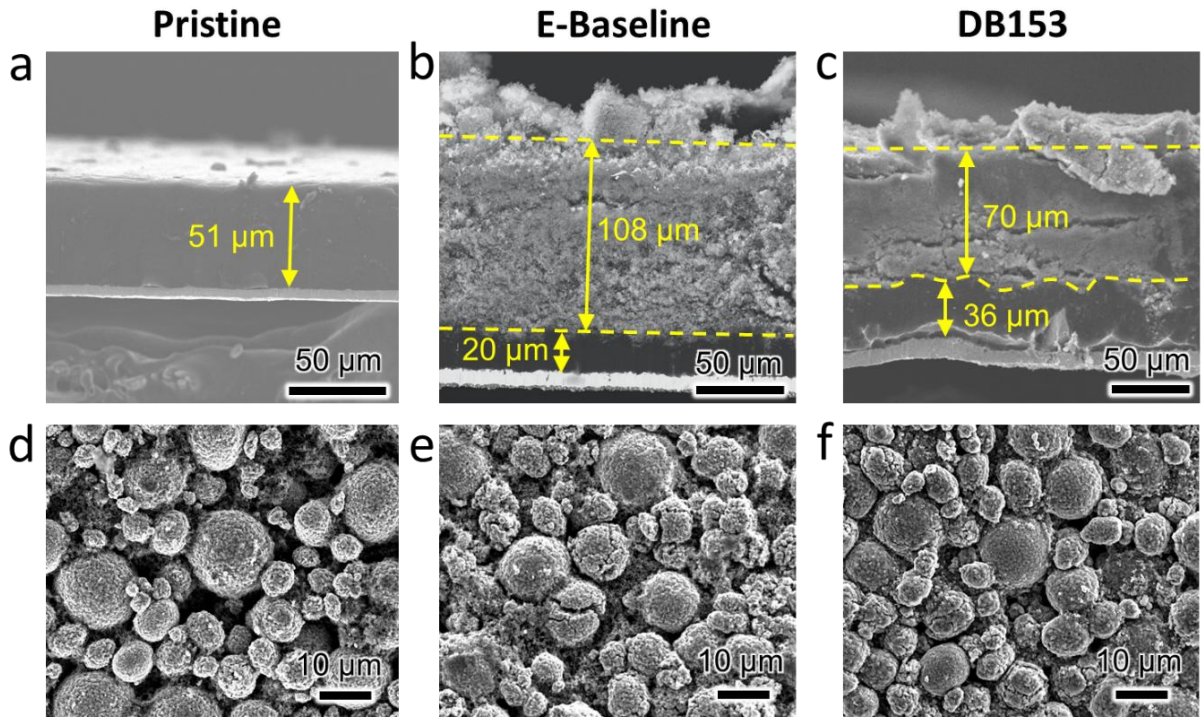

Figure S13. (a-c) Cross-section SEM image of pristine and cycled-Li anodes and (d-f) top-view SEM images of pristine and cycled-NMC811 cathodes for the E-Baseline and DB153 after 470 cycles, respectively.

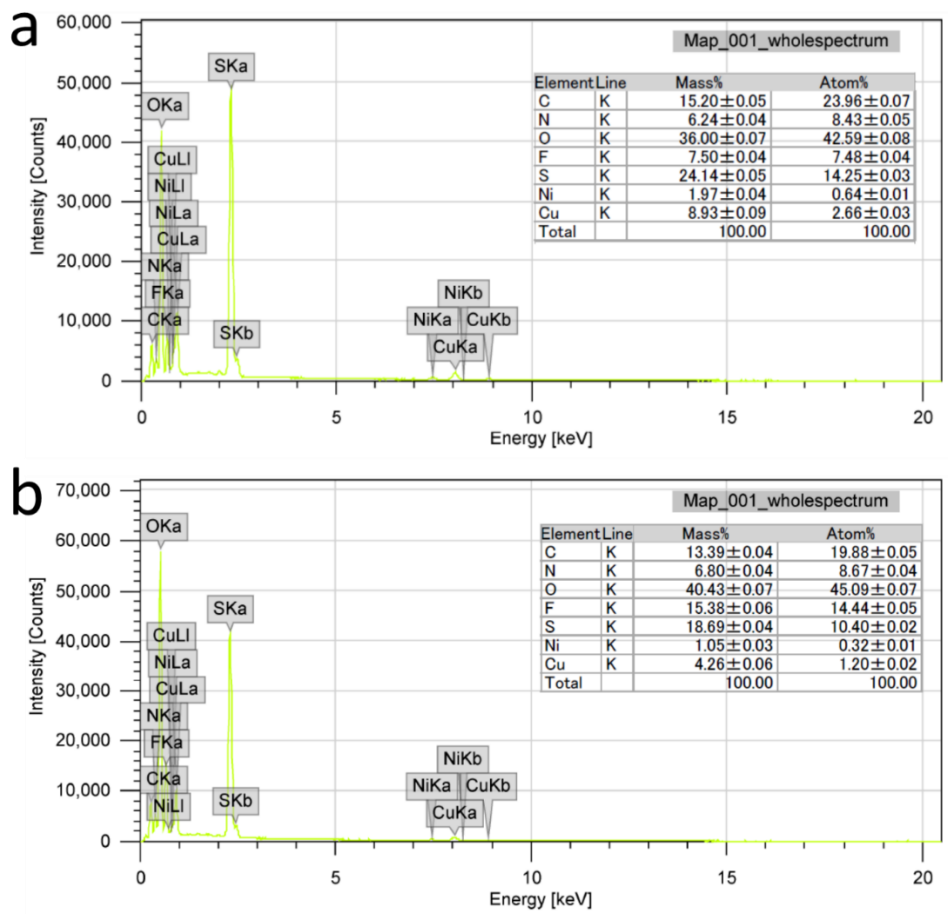

Figure S14. EDS spectra of cross-sectional cycled Li metal anode for (a) E-Baseline and (b) DB153 at the end-of-life cycle (470 cycles).

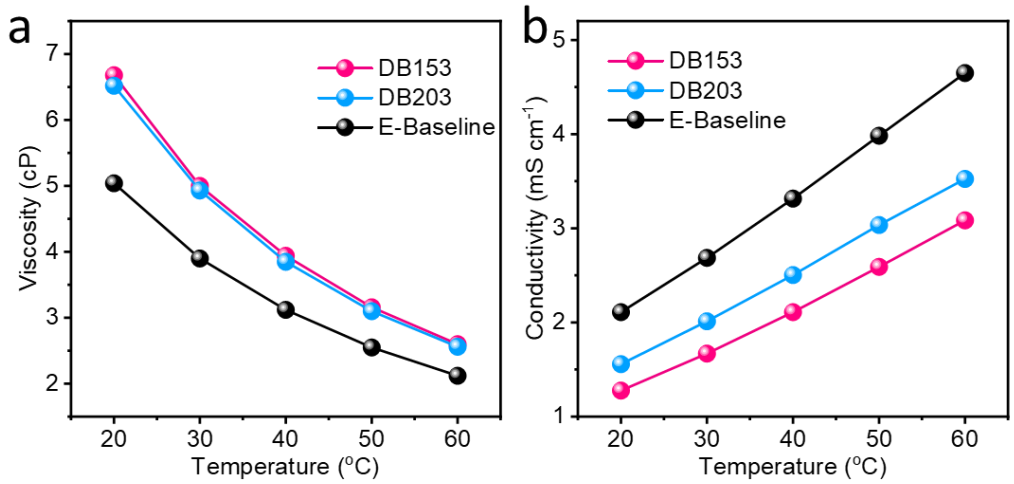

Figure S15. Temperature dependance of (a) viscosity and (b) ionic conductivity of E-Baseline (LiFSI-1.2DME-3TTE), DB203 (LiFSI-1.2DME-3BTFEE) and DB153 (LiFSI-1.15DME-3BTFEE) electrolytes.

References

[1] J. N. Canongia Lopes, A. A. H. Pádua, *J. Phys. Chem. B* **2004**, *108*, 16893.

[2] L. X. Dang, *J. Chem. Phys.* **1992**, *96*, 6970.

[3] L. S. Dodda, I. Cabeza de Vaca, J. Tirado-Rives, W. L. Jorgensen, *Nucleic Acids Res.* **2017**, *45*, W331.

[4] L. S. Dodda, J. Z. Vilseck, J. Tirado-Rives, W. L. Jorgensen, *J. Phys. Chem. B* **2017**, *121*, 3864.

[5] G. M. C. Silva, P. Morgado, P. Lourenço, M. Goldmann, E. J. M. Filipe, *Proc. Natl. Acad. Sci.* **2019**, *116*, 14868.

[6] I. V. Leontyev, A. A. Stuchebrukhov, *J. Chem. Phys.* **2009**, *130*.

[7] J. C. R. Reis, I. M. S. Lampreia, Â. F. S. Santos, M. L. C. J. Moita, G. Douhéret, *ChemPhysChem* **2010**, *11*, 3722.

[8] F. Comelli, S. Ottani, R. Francesconi, C. Castellari, *J. Chem. Eng. Data* **2002**, *47*, 1226.

[9] D. D. COFFMAN, M. S. RAASCH, G. W. RIGBY, P. L. BARRICK, W. E. HANFORD, *J. Org. Chem.* **1949**, *14*, 747.

[10] G. Bussi, D. Donadio, M. Parrinello, *J. Chem. Phys.* **2007**, *126*.

[11] H. J. C. Berendsen, J. P. M. Postma, W. F. van Gunsteren, A. DiNola, J. R. Haak, *J. Chem. Phys.* **1984**, *81*, 3684.

[12] S. Nosé, *J. Chem. Phys.* **1984**, *81*, 511.

[13] T. Darden, D. York, L. Pedersen, *J. Chem. Phys.* **1993**, *98*, 10089.

[14] B. Hess, H. Bekker, H. J. C. Berendsen, J. G. E. M. Fraaije, *J. Comput. Chem.* **1997**, *18*, 1463.

[15] W. Humphrey, A. Dalke, K. Schulten, *J. Mol. Graph.* **1996**, *14*, 33.

[16] X. Cao, P. Gao, X. Ren, L. Zou, M. H. Engelhard, B. E. Matthews, J. Hu, C. Niu, D. Liu, B. W. Arey, C. Wang, J. Xiao, J. Liu, W. Xu, J. G. Zhang, *Proc. Natl. Acad. Sci. U. S. A.* **2021**, *118*, 1.

[17] M. Valiev, E. J. Bylaska, N. Govind, K. Kowalski, T. P. Straatsma, H. J. J. Van Dam, D. Wang, J. Nieplocha, E. Apra, T. L. Windus, W. A. de Jong, *Comput. Phys. Commun.* **2010**, *181*, 1477.

[18] A. Klamt, G. Schüürmann, *J. Chem. Soc., Perkin Trans. 2* **1993**, 799.